Three-dimensional image surface acquisition in vertebrate paleontology: A review of principal techniques

ALEJANDRO OTERO[1,2]

AGUSTÍN PÉREZ MORENO[1,3]

PETER L. FALKINGHAM[4]

GUILLERMO CASSINI[1,5,6]

AGUSTÍN RUELLA[2]

MARIANO MILITELLO[1,2]

NÉSTOR TOLEDO[1,2]

1.Consejo Nacional de Investigaciones Científicas y Técnicas (CONICET).

2.División Paleontología de Vertebrados, Anexo Laboratorios, Facultad de Ciencias Naturales y Museo. Av. 122 y 60, B1900FWA La Plata, Argentina.

3.Museo Paleontológico "Egidio Feruglio". Av. Fontana 140, U9100GYO Trelew, Argentina.

4.School of Biological and Environmental Sciences, Liverpool John Moores University. Bryom Street, L3 3AF Liverpool, UK.

5.División Mastozoología, Museo Argentino de Ciencias Naturales "Bernardino Rivadavia". Av. Ángel Gallardo 470, C1405DJR Ciudad Autónoma de Buenos Aires, Argentina.

6.Departamento de Ciencias Básicas, Universidad Nacional de Luján. Ruta Nacional 5 y Av. Constitución, B6700 Luján, Argentina.

THREE-DIMENSIONAL IMAGE SURFACE ACQUISITION IN VERTEBRATE PALEONTOLOGY: A REVIEW OF PRINCIPAL TECHNIQUES

ALEJANDRO OTERO[1,2], AGUSTÍN PÉREZ MORENO[1,3], PETER L. FALKINGHAM[4], GUILLERMO CASSINI[1,5,6], AGUSTÍN RUELLA[2], MARIANO MILITELLO[1,2], AND NÉSTOR TOLEDO[1,2]

[1]Consejo Nacional de Investigaciones Científicas y Técnicas (CONICET).

[2]División Paleontología de Vertebrados, Anexo Laboratorios, Facultad de Ciencias Naturales y Museo. Av. 122 y 60, B1900FWA La Plata, Argentina. *alexandros.otero@gmail.com*; *marianomilitello@hotmail.com*; *museo3d@fcnym.unlp.edu.ar*; *ntoledo.biol@gmail.com*

[3]Museo Paleontológico "Egidio Feruglio". Av. Fontana 140, U9100GYO Trelew, Argentina. *aperezmoreno@mef.org.ar*

[4]School of Biological and Environmental Sciences, Liverpool John Moores University. Bryom Street, L3 3AF Liverpool, UK. *p.l.falkingham@ljmu.ac.uk*

[5]División Mastozoología, Museo Argentino de Ciencias Naturales "Bernardino Rivadavia". Av. Ángel Gallardo 470, C1405DJR Ciudad Autónoma de Buenos Aires, Argentina. *gcassini@macn.gov.ar*

[6]Departamento de Ciencias Básicas, Universidad Nacional de Luján. Ruta Nacional 5 y Av. Constitución, B6700 Luján, Argentina.

Abstract. Three-dimensional (3D) surface scanning includes techniques of image acquisition and image processing. Among the former, hardware devices (*e.g.*, portable and non-portable scanners, camera) capture images from the target, whereas image processing is conducted via specialized software, in which acquired images are processed to merge them into a single 3D surface model. Image surface scanning comprises a wide variety of devices which incorporate different image acquisition techniques, all of them with potential high standards results. We describe four different scanning devices and techniques commonly used in vertebrate paleontology in order to compare them in terms of pros and cons, considering different variables, such as scanning time, post-processing time, costs and image resolution. The decision on which device to choose will depend on the budget available, the portability as well as the nature of the fossil material being analyzed (*e.g.*, size, weight, accessibility). In the light of this, photogrammetry constitutes the image surface technique which fulfills these requirements, having the best cost-benefit relationship.

Key words. Fossils. Laser. Photos. Software. Post-processing.

Resumen. ADQUISICIÓN DE IMÁGENES EN TRES DIMENSIONES MEDIANTE ESCANEO DE SUPERFICIE EN PALEONTOLOGÍA DE VERTEBRADOS: REVISIÓN DE TÉCNICAS PRINCIPALES. El escaneo de superficie incluye técnicas de adquisición de imágenes y su procesamiento. La adquisición se lleva a cabo a través de diferentes dispositivos (*e.g.*, escáneres portables y fijos, cámaras) que capturan imágenes del objetivo, mientras que el procesamiento se realiza a través de software especializado en el cual las imágenes adquiridas son procesadas para fusionarlas en una imagen simple en tres dimensiones. El escaneo en 3D en paleontología de vertebrados incluye una gran variedad de dispositivos que incorporan diferentes técnicas de adquisición de imágenes, los cuales son descriptos y comparados aquí, en términos de sus ventajas y desventajas, considerando el tiempo de escaneo y post-procesamiento, costos y calidad de imagen. La decisión de qué dispositivo elegir dependerá, principalmente, del presupuesto, la transportabilidad y de la naturaleza del material fósil a ser escaneado (*e.g.*, tamaño, peso, accesibilidad). En este sentido, la fotogrametría constituye la técnica de escaneo de superficie que posee la mejor relación costo-beneficio.

Palabras clave. Fósiles. Láser. Fotos. Software. Post-procesamiento.

THE USING of three-dimensional (3D) imaging has become a widespread trend in vertebrate paleontology since the pioneer works on this field, about 20 years ago (*e.g.*, Brochu, 2000; Rayfield *et al.*, 2001; Hutchinson and García, 2002; Breithaupt *et al.*, 2004; Wilhite, 2003, 2005; Witmer, 2004; Matthews *et al.*, 2006; Sereno *et al.*, 2007). 3D digitization allows studying a variety of topics, from biomechanics of lo-comotion (*e.g.*, Hutchinson *et al.*, 2005; Gatesy *et al.*, 2009; Manning *et al.*, 2009; Mallison, 2010; Bates and Schachner, 2012; Maidment *et al.*, 2014; Reiss and Mallison, 2014; White *et al.*, 2015; Brassey *et al.*, 2017; Otero *et al.*, 2017, 2019; Sellers *et al.*, 2017; Klinkhamer *et al.*, 2018a,b), feeding modes (*e.g.*, Degrange *et al.*, 2010; Hernesniemi *et al.*, 2011; Young *et al.*, 2012; Sharp, 2014; Cuff and Rayfield,

2015; Lautenschlager *et al.*, 2016; Konietzko-Meier *et al.*, 2018), and also trackways (*e.g.*, Bates *et al.*, 2009; Falkingham *et al.*, 2009, 2014, 2018; Falkingham and Gatesy, 2014), without the need to manipulate large, heavy and fragile bones, through the production of simulations.

3D imaging of fossils including internal structure information (whole 3D imaging) can be achieved via computer-aided X-ray tomography (CT; *e.g.*, Brochu, 2002; Domínguez Alonso *et al.*, 2004; Sereno *et al.*, 2007; Paulina-Carabajal *et al.*, 2014; Knoll *et al.*, 2015; Stocker *et al.*, 2016). Whereas CT Scanning demands the researcher take the fossil specimens to the scanning device facility (*i.e.*, medical tomograph, micro-tomograph, synchroton microCT), surface scanning can be achieved by means of portable devices, which can be taken where the fossils are housed or even to the field where the fossils are still *in situ* (*e.g.*, Wilhite, 2003; Vizcaíno *et al.*, 2011; Falkingham and Gatesy, 2014; Xing *et al.*, 2016; Otero *et al.*, 2017). Ultimately, the nature of the fossil material being analyzed (*e.g.*, size, weight, accessibility) and the purpose of the study to be undertaken (*i.e.*, with or without internal structure information) will determine the final choice of either whole or surface 3D imaging.

In general, 3D surface scanning includes the techniques of image acquisition and image processing. The former is conducted via any kind of hardware device (*e.g.*, scanner, photographic digital camera), and the latter via specialized software, in which acquired images are processed to merge into a single 3D surface model in different formats (*e.g.*, .ply, .obj, .stl).

Here we present a compilation of surface scanning techniques for 3D acquisition most-commonly used in vertebrate paleontology, discussing their scope and limitations in terms of image resolution, portability, scanning time, post-processing time, and costs.

A summary of the different scanning techniques and devices involved are presented in Table 1.

Articulated arm

Today one of the most used devices to obtain 3D landmarks to perform geometric morphometrics is the MicroScribe®, based on an articulate-arm CMM (coordinate measurement machines) (Fig. 1.1), incorporating different models, each of them having two maximum work sphere diameters. Most advanced arm models present five or six degrees of freedom (DOF; translation and rotation in three perpendicular axes), also incorporating 3D laser scanner to digitize surfaces. Thus, the articulated arm can be either useful for 3D landmarks acquisition (*e.g.*, Milne *et al.*, 2009; Couette and White, 2010; Cassini, 2013) and to obtain 3D images as well (*e.g.*, Wilhite, 2003).

All the scribes come with a MicroScribe® Utility Software (MUS) which connects the device to a computer via USB 1.1 or RS-232C serial port. This software utility allows exporting digitized coordinates (*i.e.*, x, y, z collected points) in real time to an American Standard Code for Information Interchange (ASCII) plain text, Microsoft Excel or Word. Matrices of 3D coordinates can be imported into morphometric software such as Morphologika©, MorphoJ©, R©, etc. Coordinates can be exported in real time also into CAD (Computer-Aided Design) 3D software (*e.g.*, AutoCAD©, Rhinoceros©, etc.), which is particularly useful to obtain mesh surfaces of non-complex objects. To obtain 3D meshes using MicroScribe®, accessory bold tips (probes) are needed. These probes have different ball sizes, which can be displaced along the specimen avoiding damage (*e.g.*, scratches occasioned by the sharp default tip). Different approaches can be followed to obtain a 3D mesh.

3D meshing. There are different ways to obtain a 3D surface from a point cloud obtained by a CMM. All of them share the fundamentals, first obtain the 3D coordinate point cloud over the specimen surface, and then obtain the surface via software (see Tab. 1) for processing and editing 3D meshes (Fig. 2). We provide here some advice and procedures used for different purposes.

In the same way that for taking landmarks, it is very important to ensure that in each session (for different views) the relative position of the device and specimen must keep constant. In doing so, white clay or any other methods to immobilize the specimen are crucial. In order to digitize the complete specimen, it will take more than one session which depends mainly on the stylus accessibility to the anatomical discontinuities of the specimen, as well as the attachment sites for immobilize the specimen. For example, a skull would probably take at least two different positions relative to the device, one dorsal and one ventral, and perhaps some more. In this case, the MUS has the option of

TABLE 1 - Comparative attributes of scanning devices

Scanning device	Scanning time	(Post) processing time*	Transportability	Cost (US dollar)	Image resolution	Accuracy	Free software	Minimum system requirements
Articulated arm (MicroScribe®)	moderate to fast (depending on object complexity)	fast	yes	12000	moderate to high	0.0508–0.152 mm	MUS (file:///D:/Backup/2018/Insta-laci%C3%B3n/microscibe/mus.htm) Meshlab (http://www.meshlab.net/#); Blender (https://www.blender.org)	CPU: Intel 80486 66 MHz RAM: 32 MB Graphic card VGA OS: Win 98SE USB: 1.1/RS-232C HDD: 512 MB
Portable laser scanner (NextEngine®)	slow to very slow	moderate to slow (depending on computer GPU performance)	yes	3000	0.0635 mm	0.1–0.3 mm	Meshlab (http://www.meshlab.net/#); Blender (https://www.blender.org)	CPU: 2GHZ PC (Single Core) RAM: 2GB GPU: 128MB Graphics Card (Dedicated, non-integrated) OS: Windows XP USB: 2.0 HDD: 10GB Free Space
Photogrammetry	moderate to fast	moderate to slow (depending on computer GPU performance)	yes	low, potentially free	very high (depends on camera sensor)		Alive Vision Meshroom (https://alicevision.org/#meshroom); COLMAP (https://colmap.github.io/); VisualSFM (http://ccwu.me/vsfm/); OpenMVG (https://github.com/open-MVG/openMVG); (additional software can be found listed at https://peterfalkingham.com) Meshlab (http://www.meshlab.net/#); Blender (https://www.blender.org)	CPU: Multicore, >2GHz recommended RAM: 8GB+ (16+ recommended) GPU: modern discrete card, Nvidia CUDA compatible needed for most software, 8+GB VRAM desirable OS: Any HDD/SSD: dependent on dataset size (processing requires 2-3x disk space as photos)
Handheld scanner (Artec® Space Spider)	fast, almost real time	fast	yes	28000	0.1 mm	0.05 mm	Meshlab (http://www.meshlab.net/#); Blender (https://www.blender.org)	CPU: Intel Core i5 Multicore, >2GHz (AMD CPUs and Intel's Xeon processors are not recommended) RAM: 16 GB GPU: NVIDIA Quadro OS: Win 7 64 bit

*Relative post-processing time, considered under similar CPU characteristics.
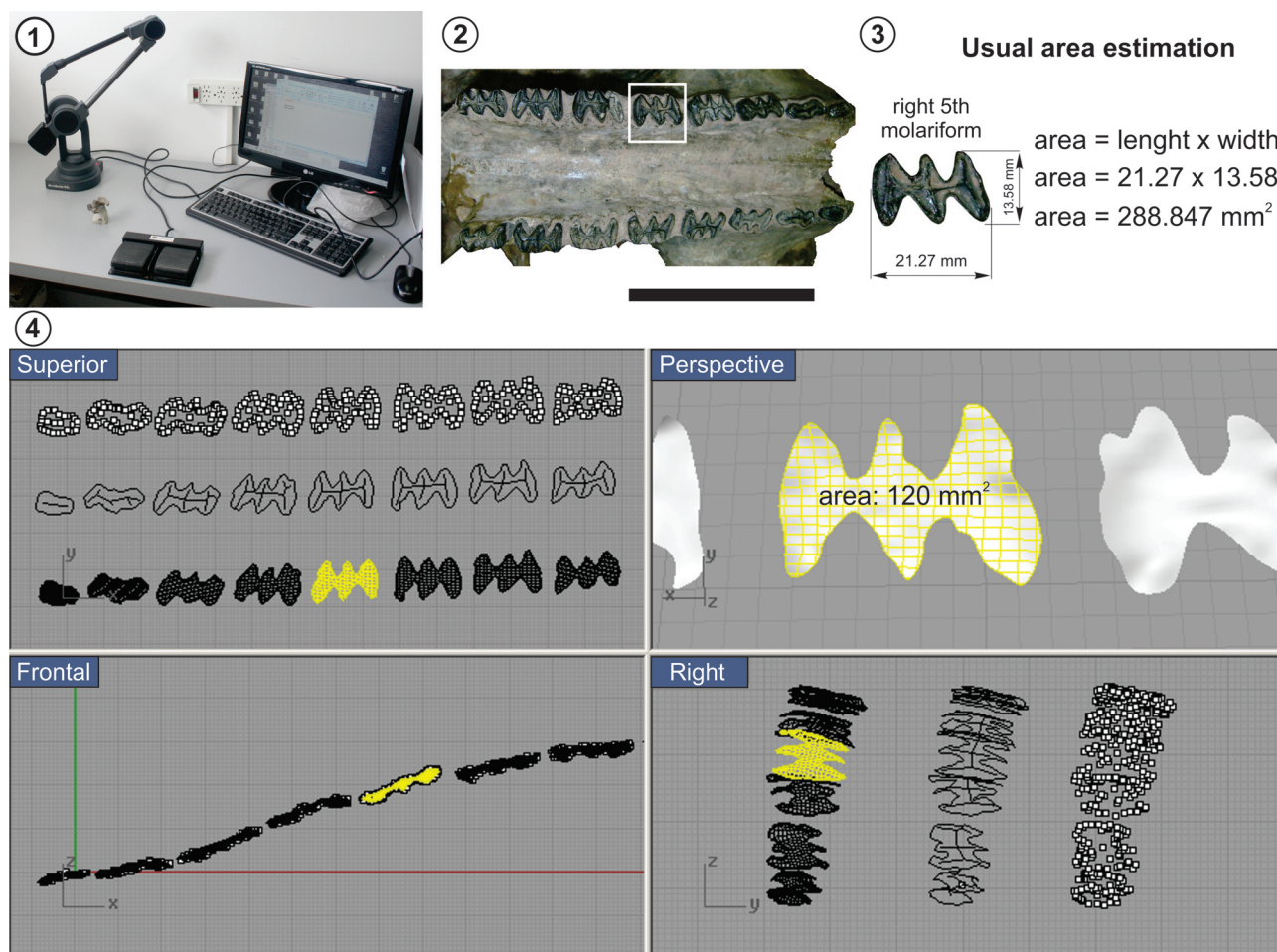
Figure 1. Tooth usual area estimation and estimation using MicroScribe® device; **1,** MicroScribe® articulated arm; **2,** dental series of the Pleistocene glyptodont *Neosclerocalyptus* (**MACN-PV 8579,** Museo Argentino de Ciencias Naturales "Bernardino Rivadavia"); **3,** usual area estimation multiplying length x width; **4,** three-dimensional area measurement using Rhinoceros© (CAD software), based on the points obtained by MicroScribe®. Command line showed area measurement and boxes: different norms from Rhinoceros© work space showing the points sampled, polylines, and reticular mesh in different views. Modified from Vizcaíno *et al.* (2016). Scale bar= 5 cm.

configure the reference frame. When used for geometric morphometric the "World Frame" is the common default used option (with the origin at the base of the articulated arm). Alternatively, a "custom frame" can be setup, in which origin, *x*-direction and *y*-direction should be taken over the same points over the specimen before each session and every time we move it respect to the CMM. This will have fixed the coordinate system in our specimen, and avoid the need for any post-processing algorithm to match the different views.

The next step is to take as many points as needed to describe the surface. At this point, many variants can be used but all share the fact that we must slide the probe tip over the specimen. In order to avoid any damage to specimen integrity (*e.g.*, scratches) an accessory probe with a bold ball at the tip must be acquired and interchanged (besides, the default tip is still needed to configure accurately the "home position" and the "custom frame"). With the proper probe, many approaches from random to planed sliding movements along the specimen surface could be used while collecting data points. It is noteworthy that unlike landmarks data, to obtain 3D surfaces the order of the digitized points is irrelevant (Fig. 2.2–3). Irrespective of movement chosen, the MUS again provide very useful options of "Auto

Scan". This function configures the MicroScribe® to automatically collect a new point at constant time interval (*e.g.*, each 2 seconds) or space displacement of the probe tip (*e.g.*, each 0.5 mm) while the user keeps pressing the measuring button.

In addition, the MUS has the option called "scan planes" which allows collecting points in slices along the surface (Fig. 2.7–9). In doing so, the user must configure the initial plane in the front of the object with three points (p1, p2, and p3), define the axis of the direction (at the back of the object) and how many planes (slices) will be used. This option is appropriated to obtain 3D meshes from quite simple surfaces (*e.g.*, long bones diaphysis, mammal's cranial rostrum and vault, etc.).

The following steps involve exporting the point cloud to a software for processing and editing 3D meshes. Some of them, as Rhinoceros© (proprietary software), allows to connect the MicroScribe® directly and import the point data at the same time we are digitizing. That approach was used by Vizcaíno *et al.* (2011) to measure the tooth occlusal surface area in glyptodonts (Fig. 1.2–4) as a tridimensional structure. When direct import of data is not possible, as in Meshlab© (http://www.meshlab.net/; Cingoni *et al.*, 2008; Ranzuglia *et al.*, 2013), the point cloud should be saved in a generic ASCII (American Standard Code for Information Interchange) point list ".txt" file (or similar) prior to be imported. At this step, these points now are interpreted as vertices, which define edges that describe faces in a polygonal mesh. In order to obtain a mesh, we first need to apply an algorithm to compute normals (*e.g.*, the compute normal for point sets in the "Normals, Curvatures and Orientation" in the MeshLab© filter menu). Selecting the option "show normal" in Render menu will help us to visualize them and adjust the parameters other than the defaults. It is noteworthy to state that the more uniform the cloud point distribution is, the easier to any algorithm to compute the vertices' normal properly (*i.e.*, when all goes in the right direction). Finally, we can obtain the mesh using the "Surface Reconstruction: Poisson" in the Remeshing, Simplification and Reconstruction option of the Filter menu of MeshLab©.

MicroScribe® systems are not cheap. The size and weight depend on the election of a system based on workspace available for digitizing, which in fact is constrained by the study object. However, as it was seeing above, there are solutions to digitize an object larger than workspace. The MicroScribe® is an excellent tool to fast capture 3D landmarks. Therefore, they are a good election to collect large samples to be analyzed by geometric morphometric methods. Although nice 3D meshes can be obtained from point data collected by a MicroScribe® (*e.g.*, Wilhite, 2003), it is not the most efficient tool since it requires time spent in the task (but see time needed by some desktop 3D scanners like NextEngine®). In addition, post-processing could be done by any CAD software that allows working with point clouds, for processing and editing 3D meshes, which, in general, do not require powerful GPU and CPU processors (except when the point clouds are extremely large) but some knowledge on 3D design. MicroScribe® arms need safe cases (*e.g.*, Pelican®) for transportation with their consequent charges by baggage weight excess, number and volume. Customs regulations when traveling between different countries could demand presentation of official documents related to the use or property of the tool. Resuming, for those people who already have a microscribe, 3D surface modeling of medium to large sized specimens could be added as a bonus function but it could not be considered as primary tool for this.

Portable laser scanner

This device is exemplified here by the NextEngine® portable scanner, composed by the proper scanner device, an auto-positioner base to hold and rotate the specimen to be scanned, and proprietary post-processing software (Fig. 3). The portable scanner captures objects in full colour with multi-laser precision, measuring 50000 points per second, which is a huge improvement respect to meshes obtained via a digitizer arm, and without the need to touch the specimen to capture the surface.

3D meshing. Three main steps can be summarized: scanning, processing, and scaling. The scanning process can be achieved through 360°, bracket or single. The first approach scans the object from every angle and the number of divisions will control the degree of rotation between scans and the total number of scans. The individual scans will be grouped as a family. The bracketing includes three consecutive angles and the number of divisions will control the
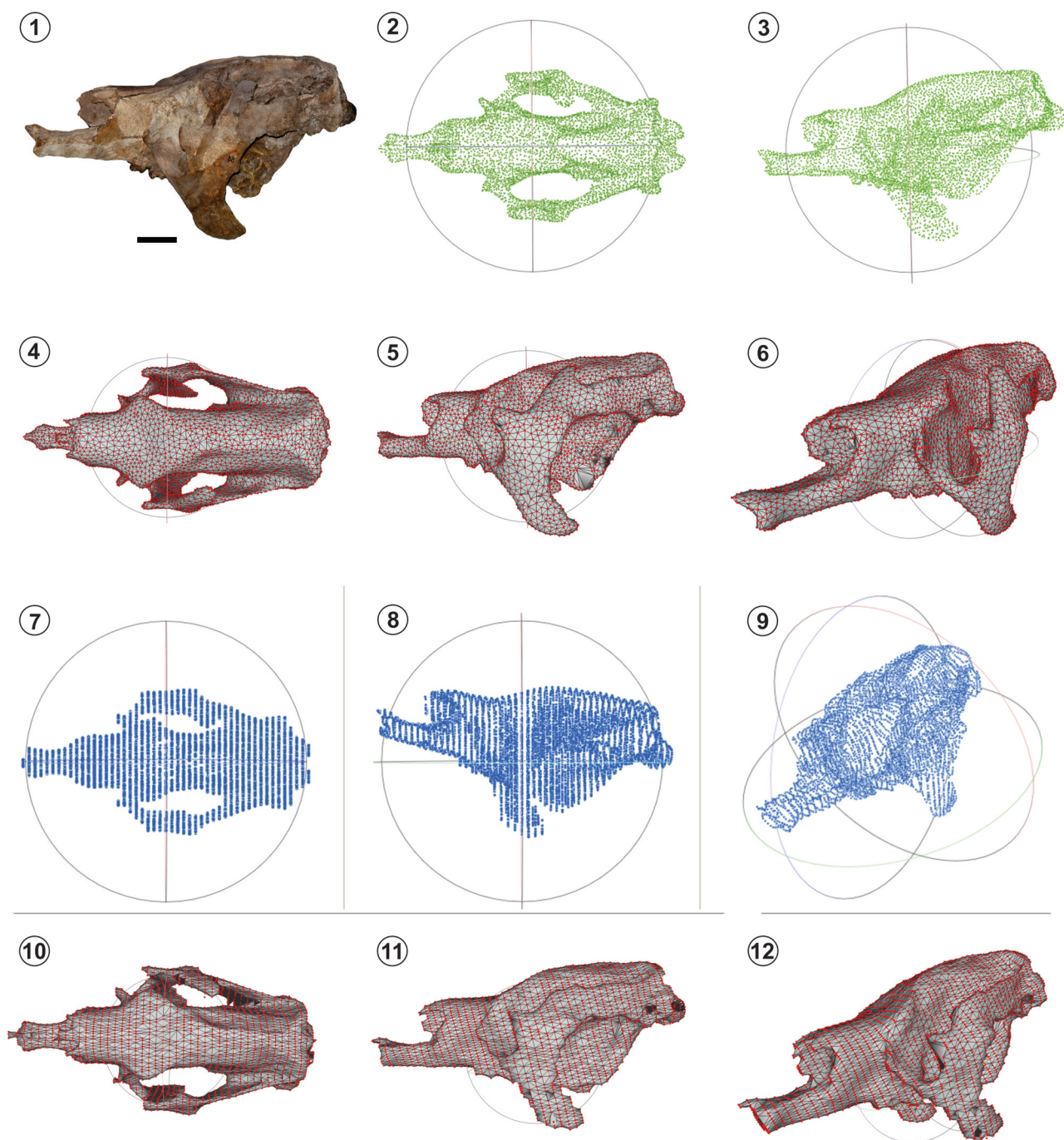
Figure 2. 3D point clouds and surface mesh from MicroScribe®. **1,** skull of *Megatherium americanum* (**MLP 2-64**) in left lateral view; **2–3,** Meshlab© screen capture from imported point cloud from a .txt file with coordinates digitized using random sliding movements (green points) in **2,** dorsal, and **3,** left lateral views; **4–6,** 3D surface mesh: with vertices (red points), faces (grey triangles) and edges (black lines) in **4,** dorsal, **5,** left lateral, and **6,** perspective views; **7–9,** Meshlab© screen capture from imported point cloud from a .txt file with coordinates digitized using "scan planes" option in MUS (blue points) in **7,** dorsal, **8,** left lateral, and **9,** perspective views; **10–12,** 3D surface mesh: with vertices (red points), faces (grey triangles) and edges (black lines) in **10,** dorsal, **11,** left lateral, and **12,** perspective views. Scale bar= 10 cm.

degree of rotation between scans. The three scans will be grouped as a family. Finally, the single scan includes only one angle scanning.

Although this scanner is provided with a fixed base where the object should be positioned, if the object to be scanned is too large, it can be positioned outside the fixed base and be scanned using a tripod and moving the scanner to cover the entire surface.

After the acquisition of a significant number of scans (*i.e*., the entire surface covered), the next step is to align all scans using the provided software (ScanStudio©, for faster processing, ScanStudio HD© is sailed separately). Alignment proceeds through the identification of homologue points (landmarks) between each scan family. Thus, it is highly recommended to include artificial landmarks (such as putty) to the fossil before the scanning to ease the aligning process (Fig. 3.2–4).

Specimens with complex structures including holes, spines, bridges, arches and blade-like parts will need extra captures to get the surface completely scanned and an additional time during alignment. Attenuation of glossy surfaces is recommended before scanning, by using of inert talc powder (a brush with talc is provided with the NextEngine®).

Finally, the 3D models generated by ScanStudio HD© can be exported as .stl, .obj, .vrml, .xyz and other formats, and imported into design software like SolidWorks©, Autodesk© 3ds Max©, Rhinoceros©, among others. As 3D models are generated with high resolution, the latter can be reduced using "Quadric Edge Collapse Decimation" in the Remeshing, Simplification and Reconstruction option of the Filter menu of MeshLab©.

Portable desktop Laser Scanners are not expensive, and a significant part of the cost is comprised in the proprietary software needed to run the scanning and built and export the models. Capture and post-processing times are large, which is a limit factor when visiting collections. Although the size is a bit smaller than a digitizer arm, a safe case is needed for transportation (*e.g*., Pelican® 72 x 44 x 27 cm).

Handheld 3D scanners

Handheld 3D scanners (Fig. 4) are gaining popularity in this fast-growing market, because they offer flexibility and

allow the 3D capture of complex objects. Several types of handheld scanning systems are available, but all share the same disadvantages: their high cost due to a high purchase
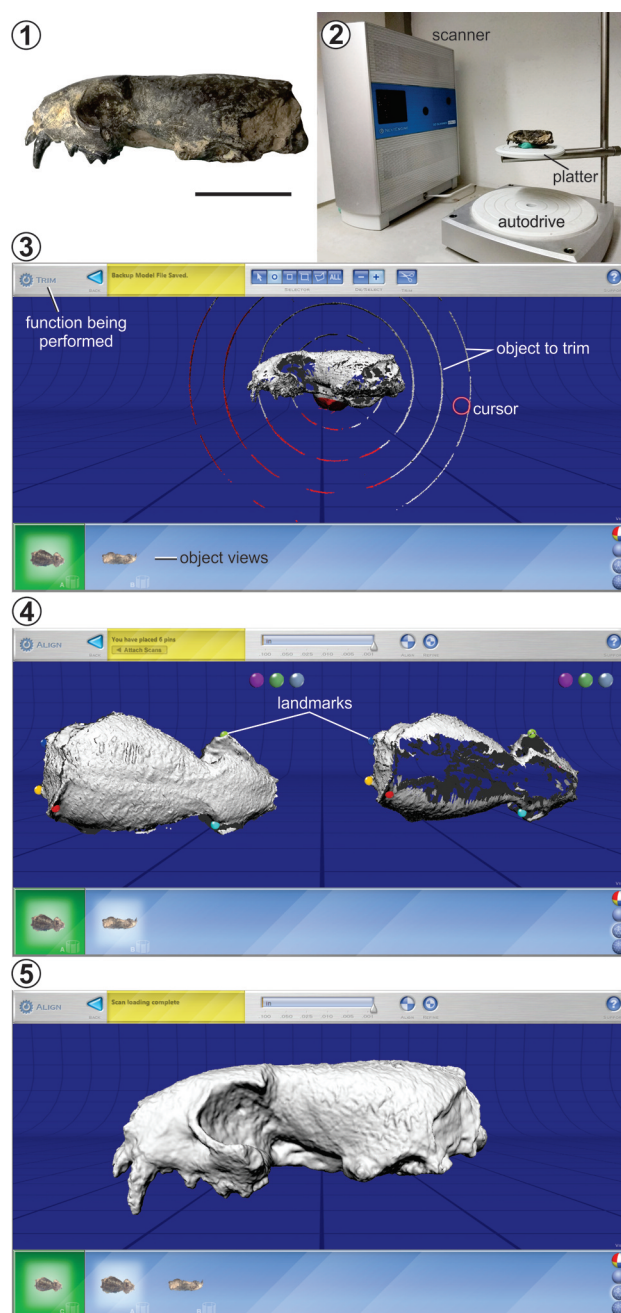

Figure 3. NextEngine® portable scanner and ScanStudio© functions; **1,** skull of *Lyncodon bosei* (**MLP 54-III-5-1**) in left lateral view; **2,** NextEngine® parts and fossil mounted; **3,** trim (*i.e*., prune) function; **4,** align function; **5,** merged mesh. Scale bar= 2 cm.

price and powerful computers to acquire and handle the pictures. However, these disadvantages are relative when compared to the large number of advantages, including fast image capture and high transportability.

The properties to be taken into account to know why this technology adds more and more followers, includes its image mode, the average density of the mesh in the scanned area, the average time of acquisition of meshes, the precision, and the post processing. Currently, these types of scanners have shown that they are capable of generating meshes as dense as those formed from CT slices, but in a tenth of the time and without the need for assistance of a highly qualified technician. The fundamental principle from which these scanners operate is the
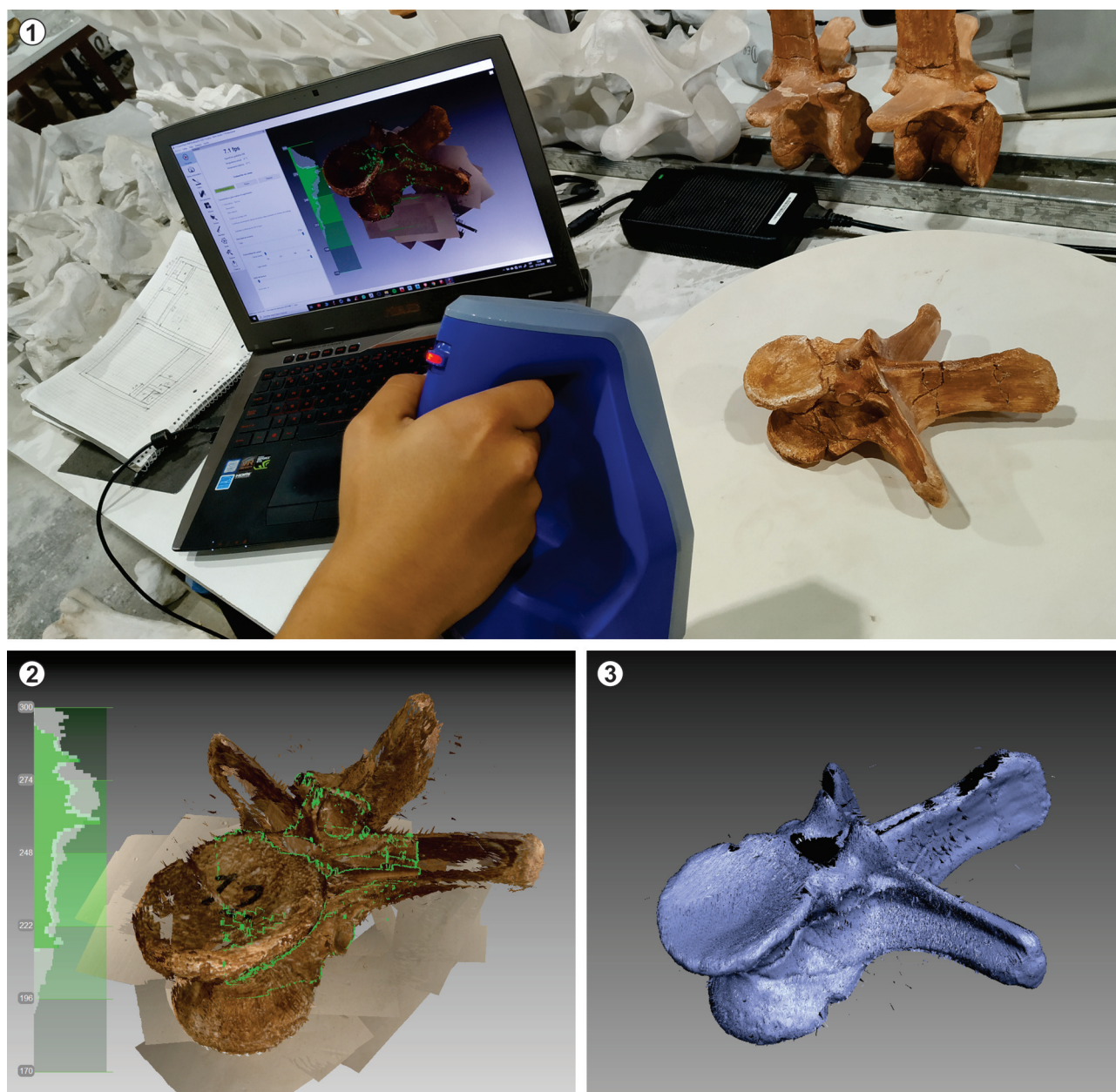
Figure 4. 1–3, Artec® Space Spider® handheld scanner; **1,** operation of Artec® Space Spider® handheld scanner on a vertebra; **2,** detail of the real time 3D image capture; **3,** merged mesh with no texture.

same one used by photogrammetry, namely, interpolation of matched contours and dots between images, but with an extra element: the lasers. These lasers collect the surface information, as in any other scanner, but in turn measure the optimal distance to the object needed to perform the scan.

The precision and post processing of handheld 3D scanners are subordinated to the hardware specifications of each scanner. As with computers, in which the performance is evaluated through their random-access memory (RAM), the processor or the type of hard disk, to evaluate the performance of the scanners certain requirements must be taken into account. These requirements can be summarized mainly in four items: the amount of "eyes" (high-definition cameras) and their resolution, the type of light, and the frame per second rate (FPS). Mainly what determines the precision of a handheld scanner are its "eyes". Multiple "eyes" scanners are ideal for scanning complex structures, whose volumes do not exceed 12.5 liters. The quality of the textures generated with these scanners is only surpassed by cameras with great macro power. On the other hand, for the "eye limited" scanners there are no restrictions on the volume of objects to be scanned, but they are deficient in texture issues. The latter are a great tool for large and simple objects or even small areas.

Regarding post-processing, these scanners are not different from other methods thanks to the existence of specialized software. Nevertheless, lacking of free available software can be seen as a huge disadvantage, and the necessary requirements of computers for the processing exceed those of more common computers (see Tab. 1).

Photogrammetry

Photogrammetry is a 3D digitization method that has been used in paleontology for nearly two decades (Breithaupt and Matthews, 2001; Breithaupt *et al.*, 2001; see Matthews *et al.*, 2016 for review). Initially, the method required extremely powerful specialized workstations and photographs taken according to a specific protocol. Over the last 5−10 years though, computers have become more powerful, digital cameras have increased quality of images, and algorithms have been optimized. As a result, today's pho-

tography process allows the use of photos taken with a smartphone, processed on a standard laptop or desktop computer using free software, to produce high-resolution and high-accuracy models far beyond what was possible just a few years ago (Falkingham, 2012; Mallison and Wings, 2014; Matthews *et al.*, 2016).

Because of this advancement in ease-of-use and affordability, photogrammetry is now commonly used throughout paleontology branches, being applied to trace (Bennett *et al.*, 2013; Xing *et al.*, 2016; Falkingham *et al.*, 2018), individual bones (White *et al.*, 2013), mounted skeletons (Bates *et al.*, 2016), invertebrates (Schlüter, 2016) and even entire sites or outcrops (Klein *et al.*, 2016). The method has even been applied to recreate lost fossils based on historical photographs (Falkingham *et al.*, 2014; Lallensack *et al.*, 2015), or to SEM (Scanning Electron Microscope) images to generate 3D models of microscopic specimens (Eulitz and Reiss, 2015).

Detailed descriptions of the method and best practice have been documented elsewhere (Falkingham, 2012; Mallison and Wings, 2014; Matthews *et al.*, 2016), but we provide here an up to date summary of what is needed, and best practice.

Equipment. A moderately high-powered desktop or laptop will be sufficient for most photogrammetry needs. Due to similarities in processing needs, "gaming PCs" turn out to generally be of ideal specifications for photogrammetry. Processor (CPU) speed, amount and speed of available RAM, and a discrete graphics processing unit (dGPU) will all determine processing times. With some exceptions (notably Agisoft® Metashape), most of the available photogrammetry software utilizes CUDA (Compute Unified Device Architecture), and so requires a Graphics Processing Unit (GPU) made by Nvidia®, and either Linux© or Windows© operating systems.

Digital photos can be taken with any device from a smartphone to a DSLR (Digital Single Lens Reflex) camera. Generally, more expensive cameras (and phones) will be able to take sharper, higher resolution images with less blur than cheaper equipment, though user experience with photography is also important. To maximize image quality, a full-frame DSLR with a prime lens in the 35−55 mm (50 mm lenses are recommended) range is generally ideal for most

specimens, though the small increase in image quality may not be worth the extra cost and lack of flexibility compared to a kit camera with zoom lens (zoom images can be used but not recommended). An extra effort is needed when photographing minute specimens. In macro mode, reduction of depth of field will focus only nearest part of the field, blurring the farthest parts. This hinders the computing when triangulating the cloud of points. Taking multiple captures at a single position to perform Depth of Field Bracketing

could be needed. As image pictures are the primary data on which models are constructed, ensuring their quality is the primary objective during photo sessions; then, shadows and blurry images should be avoided and having a depth of field becomes a "must due" standard. Consequently, tripods, remote shooters, annular led lighting and a turn table (for small to medium size specimens) are good accessories to achieve pretty good images than can save a substantial image post-processing.

Taking photographs. "How many photos?" is usually the first question asked by someone new to photogrammetry. Unfortunately, there is no hard number to aim for—the number needed will vary from specimen to specimen. A relatively flat footprint can be captured with as few as 3 photos, whilst a mounted dinosaur skeleton could take anywhere from 200–1000+. Generally, more photos (if taken correctly) will increase detail of the final digital model, but at the expense of increased processing time—most photogrammetry software at the time of writing takes exponentially longer as more photos are added, with diminishing returns in terms of model quality. In addition, the number of photos that programs can process depends on the RAM memory of the computer. For example, Metashape® manual indicates that the dense cloud building is the most GPU and memory consumed step. For a high quality dense cloud building, using 500 images coming from a 12 MPix camera (*i.e.*, 4000 x 3000 pixels) requires 8 Mb of RAM. These requirements are multiplicative in terms of image numbers (*i.e.*, 1000 photos need 16 GB) and exponential in terms of dense cloud quality (*e.g.*, ultra-high quality for 500 photos needs 32 GB). Photo resolution has a similar effect to increasing number of photos. Images between 16 and 20 megapixels are usually sufficient; the benefits of higher resolution images become outweighed by the increased processing time, whilst smaller images will struggle to capture the necessary detail. That being said, it is important to consider that what is unmanageably large data today may well be common in the near future. For the process to work, any given point of interest must be visible in at least 3 photos in order for its x, y, z position to be triangulated. This is best achieved by attempting to maintain an overlap between images of at least 2/3. When moving around a specimen (or using a turntable), photos should be taken
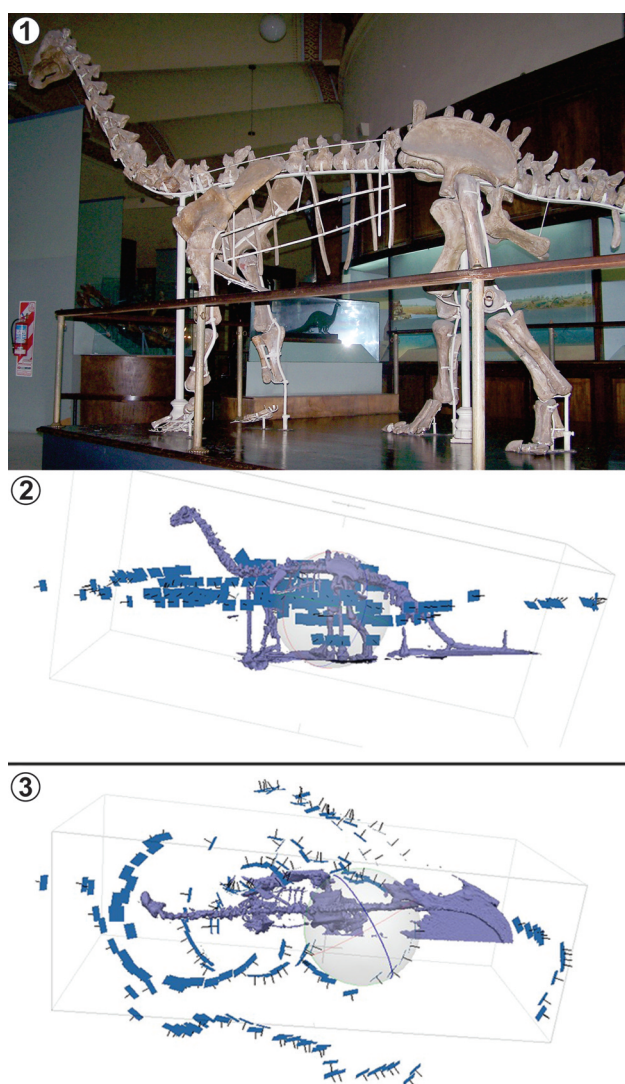
Figure 5. 1–3, taking photos for photogrammetry; **1,** *Neuquensaurus australis* mounted skeleton at Museo de La Plata; **2–3,** 3D model of *Neuquensaurus* in **2,** lateral, and **3,** dorsal views. Blue rectangles represent positions where shots were taken, whereas straight black lines on each rectangle (*i.e.*, normals) represent the focus direction.
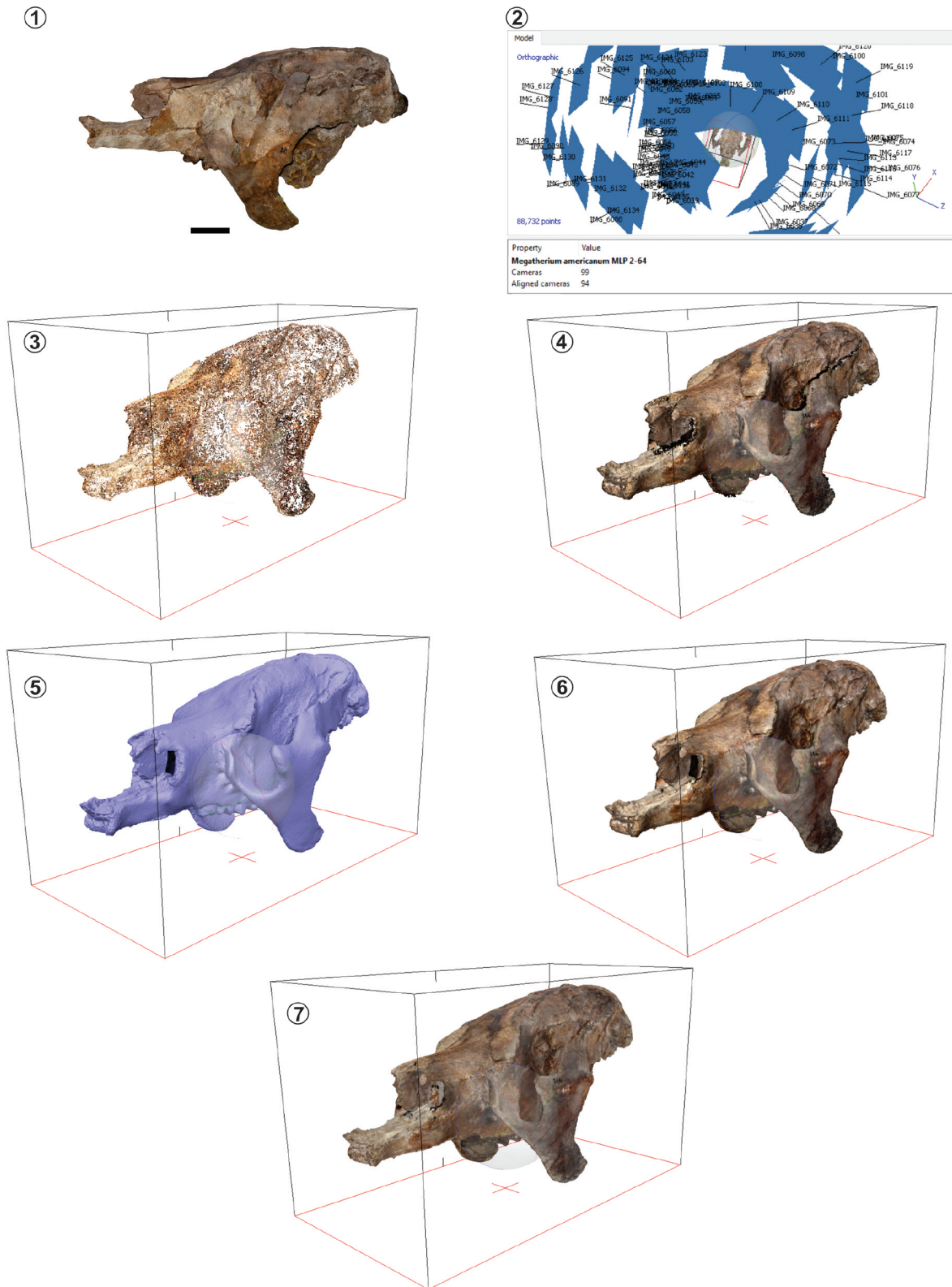
Figure 6. 1–7, general workflow for photogrammetry (example for Agisoft© Metashape©); **1,** skull of ***Megatherium americanum*** (**MLP 2-64**) in left lateral view; **2,** screen capture with align photos (each photo is represented by a blue rectangle); **3,** point cloud based on match points in aligned photos; **4,** dense cloud with coloured points; **5,** final mesh model solid view; **6,** shaded view (vertex with colours); **7,** textured mesh model. Scale bar= 10 cm.

every few degrees, resulting in ~100 photos. Taking multiple circles of photos at different heights will help with coverage. An example of camera locations for a three- dimensional specimen is shown in Figure 5. At the time of writing, 100 photos will generally take on the order of 1 hour on a modest computer from start to final textured model. A scale or any other reference object of known dimensions should be included altogether with the specimen. Matting of glossy surfaces is also recommended. Recommendations have been made elsewhere (Davies *et al.*, 2017; Falkingham *et al.*, 2018) that the model and the photographs should be archived and made available as supplemental data with any publications.

Software. The last decade has seen an explosion of available photogrammetry software packages, including a wide range of both commercial and free, open source programs. Whilst some particularly expensive solutions offer significantly decreased processing times, or easier-to-use User Interfaces (UI), most softwares are capable of similar levels of resolution and accuracy. We refrain from suggesting specific software here, because the field is changing so quickly that any recommendation made will probably be outdated by the time of publication.

The workflow consists in loading the images and then follow these steps: 1) align photos, 2) build dense cloud point, 3) build the surface mesh and 4) add the texture (Fig. 6). The result of aligning the photos is a point cloud, which can be improved cleaning the points which do not belong to the object of interest ("wrong points"). This task can be done manually or some aided by specific software with tools to do it automatically. The second step will perform better if "wrong points" were removed, generating a more accurate dense cloud. The next step is to build the mesh, and finally, although not mandatory, adding the texture to get the object digitized. Particularly, in Agisoft® Metashape® software, photos are loaded in two "chunks", each one following the above-mentioned workflow. Once the models are ready (including the texture), they must be joined. For this, all sets have to be aligned. In some software there is the option to automatically align, detecting common points or markers. Such markers can be physical markers, which are marks on the object or digital markers, which are put in a specific part of the object that the user recognize in both

photos sets using a software tool. Once sets are aligned, these can be merged to generate the final model with its texture. The final result is a complete object without blind points.

Compared with both digitizer arms and laser scanner, photogrammetry has represented an improvement in portability and budget. Given laptops and camera can be considered usual, standard equipment for most of paleontologist during work on collections or in the field, most people will already be well equipped for digitization using this method. Optionally including a tripod or turntable will round out the equipment list and enable better digitization of small or difficult specimens.

CONCLUSIONS

As depicted, the surface scanning includes a wide variety of devices which incorporate different image acquisition techniques, all of them with potential high standards results. In the light of this, the decision on which device to choose will depend on the budget available, the portability as well as the size of the target to be scanned. Considering these variables, photogrammetry constitutes the surface scanning technique which fulfils these requirements, having the best cost-benefit relationship.

REFERENCES
Bates, K.T., Falkingham, P.L., Hodgetts, J., Farlow, J.O., Breithaupt, B.H., O'Brien, M., Matthews, N., Sellers, W.I., and Manning, L. 2009. Digital imaging and public engagement in palaeontology. *Geology Today* 25: 134–139.
Bates, K.T., Mannion, P.D., Falkingham, P.L., Brusatte, S.L., Hutchinson, J.R., Otero, A., Sellers, W.I., Sullivan, C., Stevens, K., and Allen, V. 2016. Temporal and phylogenetic evolution of the sauropod dinosaur body plan. *Royal Society Open Science* 3: 150636.
Bates, K.T. and Schachner, E.R. 2012. Disparity and convergence in bipedal archosaur locomotion. *Journal of the Royal Society Interface* 9: 1339–1353.
Bennett, M.R., Falkingham, P.L., Morse, S.A., Bates, K., and Crompton, R.H. 2013. Preserving the Impossible: Conservation of soft-sediment hominin footprint sites and strategies for three-

dimensional digital data capture. *PLoS ONE* 8: e60755.

Brassey, C.A., Maidment, S.C.R., and Barrett, P.M. 2017. Muscle moment arm analyses applied to vertebrate paleontology: a case study using *Stegosaurus stenops* Marsh, 1887. *Journal of Vertebrate Paleontology* 37: e1361432.

Breithaupt, B.H. and Matthews, N.A. 2001. Preserving paleontological resources using photogrammetry and geographic information systems. In: D. Harmon (Ed.), *Crossing Boundaries in Park Management*. Proceedings of the 11th Conference on Research and Resource Management in Parks and Public Lands, The George Wright Society, Inc., p. 62–70.

Breithaupt, B.H., Matthews, N., and Noble, T. 2004. An integrated approach to three-dimensional data collection at dinosaur tracksites in the Rocky Mountain West. *Ichnos* 11: 11–26.

Breithaupt, B.H, Southwell, E.H., Adams, T., and Matthews, N.A. 2001. Innovative Documentation Methodologies in the Study of the Most Extensive Dinosaur Tracksite in Wyoming. *6th Fossil Research Conference Proceedings* (Lakewood), 113–22.

Brochu, C.A. 2000. A digitally-rendered endocast for *Tyrannosaurus rex*. *Journal of Vertebrate Paleontology* 20: 1–6.

Brochu, C.A. 2002. Osteology of *Tyrannosaurus rex*: insights from a nearly complete skeleton and high-resolution computed tomographic analysis of the skull. *Journal of Vertebrate Paleontology Memoir* 7: 1–138.

Cassini, G.H. 2013. Skull geometric morphometrics and paleoecology of santacrucian (late early Miocene; Patagonia) native ungulates (Astrapotheria, Litopterna, and Notoungulata). *Ameghiniana* 50: 193–216.

Cingoni, P., Callieri, M., Corsini, M., Dellepiane, M., Ganovelli, F., and Ranzuglia, G. 2008. MeshLab: an open-source mesh processing tool. *6th Eurographics Italian Chapter Conference* (Salerno), 129–136.

Couette, S. and White, J. 2010. 3D geometric morphometrics and missing-data. Can extant taxa give clues for the analysis of fossil primates? *Ameghiniana* 9: 423–433.

Cuff, A.R. and Rayfield, E.J. 2015. Retrodeformation and muscular reconstruction of ornithomimosaurian dinosaur crania. *PeerJ* 3: e1093.

Davies, T.G., Rahman, I.A., Lautenschlager, S., Cunningham, J.A., Asher, R.J., Barrett, P.M., Bates, K.T., Bengtson, S., Benson, R.B.J., Boyer, D.M., Braga, J., Bright, J.A., Claessens, L.P.A.M., Cox, P.G., Dong, X.P., Evans, A.R., Falkingham, P.L., Friedman, M., Garwood, R.J., Goswami, A., Hutchinson, J.R., Jeffery, N.S., Johanson, Z., Lebrun, R., Martínez-Pérez, C., Marugán-Lobón, J., O'Higgins, P.M., Metscher, B., Orliac, M., Rowe, T.B., Rücklin, M., Sánchez-Villagra, M.R., Shubin, N.H., Smith, S.Y., Starck, J.N., Stringer, C., Summers, A.P., Sutton, M.D., Walsh, S.A., Weisbecker, V., Witmer, L.M., Wroe, S., Yin, Z., Rayfield, E.J., and Donoghue, P.C.J. 2017. Open data and digital morphology. *Proceedings of the Royal Society B: Biological Sciences* 284: 20170194.

Degrange, F.J., Tambussi, C.P., Moreno, K., Witmer, L.M., and Wroe, S. 2010. Mechanical Analysis of feeding behavior in the extinct "terror bird" *Andalgalornis steulleti* (Gruiformes, Phorusrhacidae). *PLoS ONE* 5: e11856.

Domínguez Alonso, P., Milner, A.C., Ketcham, R.A., Cookson, M.J., and Rowe, T.B. 2004. The avian nature of the brain and inner ear of *Archaeopteryx*. *Nature* 430: 666–669.

Eulitz, M. and Reiss, G. 2015. 3D reconstruction of SEM images by use of optical photogrammetry software. *Journal of Structural Biology* 191: 190–96.

Falkingham, P.L. 2012. Acquisition of high resolution three-dimensional models using free, open-source, photogrammetric

software. *Palaeontologia Electronica* 15: 1T: 15p. doi.org/10.26879/264

Falkingham, P.L., Bates, K.T., Avanzini, M., Bennett, M., Bordy, E.M., Breithaupt, B.H., Castanera, D., Citton, P., Díaz-Martínez, I., Farlow, J.O., Fiorillo, A., Gatesy, S.M., Getty, P., Hatala, K.G., Hornung, J.J., Hyatt, J.A., Klein, H., Lallensack, J.N., Martin, A.J., Marty, D., Matthews, N.A., Meyer, C.A., Milàn, J., Minter, N.J., Razzolini, N.L., Romilio, A., Salisbury, S.W., Sciscio, L., Tanaka, I., Wiseman, A.L.A., Xing, L.D., and Belvedere, M. 2018. A standard protocol for documenting modern and fossil ichnological data. *Palaeontology* 61: 469–80.

Falkingham, P.L., Bates, K.T., and Farlow, J.O. 2014. Historical photogrammetry: bird's Paluxy River dinosaur chase sequence digitally reconstructed as it was prior to excavation 70 Years Ago. *PLoS ONE* 9: e93247.

Falkingham, P.L. and Gatesy, S.M. 2014. The birth of a dinosaur footprint: Subsurface 3D motion reconstruction and discrete element simulation reveal track ontogeny. *PNAS* 111: 18279–18284.

Falkingham, P.L., Margetts, L., Smith, I.A., and Manning, P.L. 2009. Reinterpretation of palmate and semi-palmate (webbed) fossil tracks; insights from finite element modelling. *Palaeogeography, Palaeoclimatology, Palaeoecology* 271: 69–76.

Gatesy, S.M., Bäker, M., and Hutchinson, J.R. 2009. Constraint-based exclusion of limb poses for reconstructing theropod dinosaur locomotion. *Journal of Vertebrate Paleontology* 29: 535–544.

Hernesniemi, E., Blomstedt, K., and Fortelius, M. 2011. Multi-view stereo three-dimensional reconstruction of lower molars of recent and Pleistocene rhinoceroses for mesowear analysis. *Palaeontologia Electronica* 14: 2T:15p. doi.palaeo-electronica.org/2011_2/246/index.html.

Hutchinson, J.R., Anderson, F.C., Blemker, S.S., and Delp, S.L. 2005. Analysis of hindlimb muscle moment arms in *Tyrannosaurus rex* using a three-dimensional musculoskeletal computer model: implications for stance, gait, and speed. *Paleobiology* 31: 676–701.

Hutchinson, J.R. and García, M. 2002. *Tyrannosaurus* was not a fast runner. *Nature* 415: 1018–1021.

Klein, H., Wizevich, M.C., Thüring, B., Marty, D., Thüring, S., Falkingham, P.L., and Meyer, C.A. 2016. Triassic chirotheriid footprints from the Swiss Alps: ichnotaxonomy and depositional environment (Cantons Wallis & Glarus). *Swiss Journal of Palaeontology* 135: 295–314.

Klinkhamer, A.J., Mallison, H., Poropat, S.F., Sinapius, G.H.K., and Wroe, S. 2018a. Three-dimensional musculoskeletal modeling of the sauropodomorph hind limb: the effect of postural change on muscle leverage. *The Anatomical Record* 301: 2145–2163.

Klinkhamer, A.J., Mallison, H., Poropat, S.F., Sloan, T., and Wroe, S. 2018b. Comparative three-dimensional moment arm analysis of the sauropod forelimb: implications for the transition to a wide-gauge stance in titanosaurs. *The Anatomical Record* 302: 794–817.

Knoll, F., Witmer, L.M., Ridgely, R.C., Ortega, F., and Sanz, J.L. 2015. A New Titanosaurian braincase from the Cretaceous "Lo Hueco" locality in Spain sheds light on neuroanatomical evolution within Titanosauria. *PLoS ONE* 10: e0138233.

Konietzko-Meier, D., Gruntmejer, K., Marcé-Nogué, J., Bodzioxh, A., and Fortuny, J. 2018. Merging cranial histology and 3D-computational biomechanics: a review of the feeding ecology of a Late Triassic temnospondyl amphibian. *PeerJ* 6: e4426.

Lallensack, J.N., Sander, P.M., Knötschke, N., and Wings, O. 2015. Dinosaur tracks from the Langenberg Quarry (Late Jurassic, Germany) reconstructed with historical photogrammetry: Evidence

for large theropods soon after insular dwarfism. *Palaeontologia Electronica* 18: 1–34.

Lautenschlager, S., Brassey, C.A., Button, D.J., and Barrett, P.M. 2016. Decoupled form and function in disparate herbivorous dinosaur clades. *Scientific Reports* 6: 26495.

Maidment, S.C.R., Bates, K.T., Falkingham, P.L., VanBuren, C., Arbour, V., and Barrett, P.M. 2014. Locomotion in ornithischian dinosaurs: an assessment using three-dimensional computational modelling. *Biological Reviews* 89: 588–617.

Mallison, H. 2010. The digital *Plateosaurus* II: An assessment of the range of motion of the limbs and vertebral column and of previous reconstructions using a digital skeletal mount. *Acta Palaeontologica Polonica* 55: 433–458.

Mallison, H. and Wings, O. 2014. Photogrammetry in paleontology - a practical guide. *Journal of Paleontological Techniques* 12: 1–31.

Manning, P.L., Margetts, L., Johnson, M.R., Withers, P.J., Sellers, W.I., Falkingham, P.L., Mummery, P.M., Barrett, P.M., and Raymont, D.R. 2009. Biomechanics of dromaeosaurid dinosaur claws: application of x-ray microtomography, nanoindentation, and finite element analysis. *The Anatomical Record* 292: 1397–1405.

Matthews, N.A., Noble, T.A., and Breithaupt, B.H. 2006. The application of photogrammetry, remote sensing and geographic information systems (GIS) to fossil resource management. *Bulletin New Mexico Museum of Natural History and Science* 34: 119–131.

Matthews, N.A., Noble, T.A., and Breithaupt, B.H. 2016. Close-range photogrammetry for 3-D Ichnology: the basics of photogrammetric ichnology. In: P.L. Falkingham, D. Marty, and A. Richter (Eds.), *Dinosaur Tracks: The Next Steps*. Indiana University Press, Bloomington, p. 29–55.

Milne, N.M., Vizcaíno, S.F., and Fernicola, J.C. 2009. A 3D geometric morphometric analysis of digging ability in the extant and fossil cingulate humerus. *Journal of Zoology* 278: 48–56.

Otero, A., Allen, V., Pol, D., and Hutchinson, J.R. 2017. Forelimb muscle and joint actions in Archosauria: insights from *Crocodylus johnstoni* (Pseudosuchia) and *Mussaurus patagonicus* (Sauropodomorpha). *PeerJ* 5: e3976.

Otero, A., Cuff, A.R., Allen, V., Sumner-Rooney, L., Pol, D., and Hutchinson, J.R. 2019. Ontogenetic changes in the body plan of the sauropodomorph dinosaur *Mussaurus patagonicus* reveal shifts of locomotor stance during growth. *Scientific Reports* 9: 7614.

Paulina-Carabajal, A., Carballido, J.L., and Currie, P.J. 2014. Braincase, neuroanatomy, and neck posture of *Amargasaurus cazaui* (Sauropoda, Dicraeosauridae) and its implications for understanding head posture in sauropods. *Journal of Vertebrate Paleontology* 34: 870–882.

Ranzuglia, G., Callieri, M., Dellepiane, M., Cignoni, P., and Scopigno, R. 2013. MeshLab as a complete tool for the integration of photos and color with high resolution 3D geometry data. *CAA 2012 Conference Proceedings* (Southampton), 406–416.

Rayfield, E.J., Norman, D.B., Horner, C.C., Horner, J.R., Smith, P.M., Thomason, J.J., and Upchurch, P. 2001. Cranial design and function in a large theropod dinosaur. *Nature* 409: 1033–1037.

Reiss, S. and Mallison, H. 2014. Motion range of the manus of *Plateosaurus engelhardti* von Meyer, 1837. *Palaeontologia Electronica* 17: 12A: 19p.

Schlüter, N. 2016. Ecophenotypic variation and developmental instability in the Late Cretaceous echinoid *Micraster brevis* (Irregularia; Spatangoida). *PLoS ONE* 11: e0148341.

Sellers, W.I., Pond, S.B., Brassey, C.A., Manning, P.L., and Bates, K.T. 2017. Investigating the running abilities of *Tyrannosaurus rex* using stress-constrained multibody dynamic analysis. *PeerJ* 5: e3420.

Sereno, P.C., Wilson, J.A., Witmer, L.M., Whitlock, J.A., Maga, A., Ide, O., and Rowe, T.A. 2007. Structural extremes in a cretaceous dinosaur. *PLoS ONE* 2: e1230.

Sharp, A.C. 2014. Three dimensional digital reconstruction of the jaw adductor musculature of the extinct marsupial giant *Diprotodon optatum*. *PeerJ* 2: e514.

Stocker, M.R., Nesbitt, S.J., Criswell, K.E., Parker, W.G., Witmer, L.M., Rowe, T.B., Ridgely, R., and Brown, M.A. 2016. A dome-headed stem archosaur exemplifies convergence among dinosaurs and their distant relatives. *Current Biology* 26: 2674–2680.

Vizcaíno, S.F., Cassini, G.H., Fernicola, J.C., and Bargo, M.S. 2011. Evaluating habitats and feeding habits through ecomorphological features in glyptodonts (Mammalia, Xenarthra). *Ameghiniana* 48: 305–319.

Vizcaíno, S.F., Bargo, M.S., Cassini, G.H., and Toledo, N. 2016. *Forma y función en Paleobiología de Vertebrados*. EDULP, La Plata, 268 p.

White, M.A., Bell, P.R., Cook, A.G., Barnes, D.G., Tischler, T.R., Bassam, B.J., and Elliott, D.A. 2015. Forearm range of motion in *Australovenator wintonensis* (Theropoda, Megaraptoridae). *PLoS ONE* 10: e0137709.

White, M.A., Falkingham, P.L., Cook, A.G., Hocknull, S.A., and Elliott, D.A. 2013. Morphological comparisons of metacarpal I for *Australovenator wintonensis* and *Rapator ornitholestoides*: implications for their taxonomic relationships. *Alcheringa* 37: 435–41.

Wilhite, D.R. 2003. [*Biomechanical reconstruction of the appendicular skeleton in three North American Jurassic Sauropods*. Ph. Dissertation, Louisiana State University, Baton Rouge, 185 p. Unpublished.].

Wilhite, D.R. 2005. Variation in the appendicular skeleton of North American sauropod dinosaurs: taxonomic implications. In: V. Tidwell, and K. Carpenter (Eds.), *Thunder lizards: the sauropodomorph dinosaurs*. Indiana University Press, Bloomington, p. 268–302.

Witmer, L.M. 2004. Inside the oldest bird brain. *Nature* 430: 619–620.

Xing, L., Li, D., Falkingham, P.L., Lockley, M.G., Benton, M.J., Klein, H., Zhang, J., Ran, H., Persons, S., and Dai, H. 2016. Digit-only sauropod pes trackways from China - evidence of swimming or a preservational phenomenon? *Scientific Reports* 6: 21138.

Young, M.T. Rayfield, E.J., Holliday, C.M., Witmer, L.M., Button, D.J., Upchurch, P., and Barrett, P.M. 2012. Cranial biomechanics of *Diplodocus* (Dinosauria, Sauropoda): testing hypotheses of feeding behavior in an extinct megaherbivore. *Naturwissenschaften* 99: 637–643.